

Density fluctuations in molten salts. I. Inelastic neutron scattering from liquid RbBr[†]

D. L. Price

Solid State Science Division, Argonne National Laboratory, Argonne, Illinois 60439

J. R. D. Copley

*Solid State Science Division, Argonne National Laboratory, Argonne, Illinois 60439
and Institut Laue-Langevin, B.P. 156 Centre de Tri, 38042 Grenoble Cedex, France*

(Received 27 February 1975)

The density fluctuations in molten salts are being investigated with a combination of neutron-scattering and computer-simulation techniques. In this paper results are given for measurements of the coherent inelastic neutron scattering from molten RbBr at 986 K, in the wave-vector range $1 \lesssim Q \lesssim 7 \text{ \AA}^{-1}$. In view of the similarity between the Rb⁺ and Br⁻ ions with regard to size, mass, and neutron scattering length, the scattering function measured in these experiments closely reflects the behavior of the number density fluctuations in the melt, regardless of ion type.

I. INTRODUCTION

The problem of interpreting the dynamical behavior of the atoms in a liquid in terms of interatomic potentials is more complicated than in the case of a gas or a crystalline solid, where simple starting approximations exist. In recent years, however, considerable progress has been made for the simplest liquids, by making detailed comparisons between the results of inelastic neutron-scattering measurements and those of computer simulations of appropriate model systems. Liquid argon^{1, 2} and liquid rubidium^{3, 4} have been extensively studied using both techniques. In both cases the computer simulation (generally known as "molecular dynamics") gives results in good agreement with the neutron data, when the interactions between atoms (neutral "pseudoatoms" in the metallic case) are represented by a single two-body interaction potential $\phi(r)$. Moreover, the argon and rubidium data are qualitatively similar, when appropriate scaling is applied to the distance and time variables, except in the region of small momentum transfer $Q \lesssim 1 \text{ \AA}^{-1}$, where qualitatively different behavior between the two types of liquid is observed in both the neutron-scattering experiments^{5, 6} and the molecular-dynamics calculations.^{2, 7}

The present work represents an extension of this two-fold approach to the case of a molten salt. It is an extension in two senses, in that (a) two atomic species are involved, and (b) strong Coulomb attractive forces between ions of different type are present. In contrast, the weak attractive forces between atoms in liquefied inert gases and in metals are caused by polarization effects. The most obvious way to examine effects due to the presence of two atomic species would be to study a mixture of liquefied rare gases or else an alloy

of two alkali metals. In the present study we have instead focused our attention on effects due to the Coulomb attractive forces. We have chosen rubidium bromide for the experiment because the Rb⁺ and Br⁻ ions are similar in both mass and radius (Table I). Under these conditions the Rb⁺-Rb⁺ and Br⁻-Br⁻ potentials are quantitatively similar (see Fig. 1) and to a good approximation the motions of the ions are just governed by the (common) potential between like ions and by the potential between unlike ions.

A second consideration relates to the form of the measured scattering from an alkali halide. In the most general case the scattering cross section includes three coherent components and two incoherent components (see Sec. II). Since the incoherent neutron-scattering cross sections of Rb and Br are both small (see Table I), we may to a good approximation neglect the incoherent components. Furthermore, the similarity of the two potentials between like types of ion allows us to

TABLE I. Parameters for Rb⁺ and Br⁻ ions.

	Rb ⁺	Br ⁻
Charge (units of $ e $)	1	-1
Ionic radius ^a (Å)	1.66	1.79
Mass (amu)	85.47	79.90 ₄
Nuclear scattering length (10 ⁻¹² cm)	0.685 ± 0.01 ^b	0.683 ± 0.005 ^c
Incoherent scattering cross section (b)	0.003 ^d	0.24 ± 0.24 ^e

^aSee Ref. 9, Table 3.

^bJ. R. D. Copley, *Acta Crystallogr.* **A26**, 376 (1970).

^cG. E. Bacon (unpublished).

^dS. J. Cocking, *Adv. Phys.* **16**, 189 (1967).

^eValue based on the total cross section, 6.1 ± 0.2 b, listed in *Neutron Cross Sections*, BNL Report No. 325, compiled by D. J. Hughes and R. B. Schwartz (U. S. GPO, Washington, D.C., 1958), second ed.

write the cross section in terms of only two scattering functions $S(Q, \omega)$. Thus we write the double differential scattering cross section, per unit solid angle Ω and unit of scattered energy E_1 , as

$$\frac{d^2\sigma}{d\Omega dE_1} \propto (b_1^2 + b_2^2)S_l(Q, \omega) + 2b_1 b_2 S_u(Q, \omega).$$

Here the subscripts l and u refer to like and unlike types of ion, b_1 and b_2 are the scattering amplitudes of the two types of ion, and $\hbar\omega$ denotes energy transfer. In order to extract S_l and S_u it is necessary to perform two experiments, using nuclei with different ratios b_1/b_2 . (Note that in the most general case five separate experiments would be required in order to determine the five scattering functions S_{11} , S_{12} , S_{22} , S_1^s , and S_2^s — see Sec. II).

It is often useful to consider the functions $S_{NN} \equiv S_l + S_u$ and $S_{QQ} \equiv S_l - S_u$, rather than the functions S_l and S_u , as discussed in Sec. II. Since Rb and Br have essentially identical scattering lengths (Table I), the scattering from RbBr depends only on $S_{NN}(Q, \omega)$, which describes the density fluctuations, regardless of ion type. It is therefore meaningful to compare the results of an experiment on RbBr with those obtained from monatomic liquids such as argon and rubidium.

In order to obtain $S_{QQ}(Q, \omega)$ in a single experiment, one must choose isotopes such that $b_1 + b_2 \approx 0$. This condition can only be achieved with difficulty, using $^7\text{Li}^{37}\text{Cl}$ for example, but in this case the approximation $S_{11}(Q, \omega) \approx S_{22}(Q, \omega)$ is no longer likely to be valid. Nevertheless, it would be interesting to see such an experiment performed. Alternatively $S_{QQ}(Q, \omega)$ can be obtained by performing a series of experiments with isotopes with different scattering lengths, but this is both difficult and time consuming. In the meantime one can study the results of molecular-dynamics experiments, in which the individual scattering functions are obtained simultaneously. The results of such an experiment are reported in a forthcoming paper,⁸ hereafter referred to as II.

The interatomic potentials for RbBr, derived from the work of Tosi and Fumi⁹ (see also II), are shown in Fig. 1. The potentials for Ar and Rb, scaled in energy and distance, are also shown for comparison. This figure leads one to expect that the scattering functions for Ar and Rb will be similar and that the scattering function of RbBr will be rather different from these two: such is indeed the case.

In the following section we define the scattering functions for a multicomponent system, and quote some useful results for later use both in this paper and in II. The measurements and the data reduction procedure are described in Sec. III, and

Sec. IV contains the results of the experiment. A detailed comparison with the results of earlier experiments^{1, 3} on Ar and Rb will be presented in a later paper.

II. DEFINITIONS

The double differential scattering cross section per atom, for a system with n types of atom, may be written as

$$\frac{d^2\sigma}{d\Omega dE_1} = \left. \frac{d^2\sigma}{d\Omega dE_1} \right|_{\text{coh}} + \left. \frac{d^2\sigma}{d\Omega dE_1} \right|_{\text{inc}} \quad (1)$$

where the coherent and incoherent cross sections are given by

$$\left. \frac{d^2\sigma}{d\Omega dE_1} \right|_{\text{coh}} = \frac{1}{\hbar N} \frac{k_1}{k_0} \sum_A^n \sum_B^n \langle b_A \rangle \langle b_B \rangle (N_A N_B)^{1/2} S_{AB}(\vec{Q}, \omega) \quad (2a)$$

and

$$\left. \frac{d^2\sigma}{d\Omega dE_1} \right|_{\text{inc}} = \frac{1}{\hbar N} \frac{k_1}{k_0} \sum_A^n (\langle b_A^2 \rangle - \langle b_A \rangle^2) N_A S_A^s(\vec{Q}, \omega), \quad (2b)$$

respectively. Here N_A , $4\pi\langle b_A \rangle^2$, and $4\pi\langle b_A^2 \rangle$ are the number of atoms of type A , and the coherent and total scattering cross sections per atom of type A , respectively. $N \equiv \sum_A^n N_A$ is the total number of atoms, and \vec{k}_0 and \vec{k}_1 are the incident and scattered neutron wave vectors, respectively. The partial scattering functions $S_{AB}(\vec{Q}, \omega)$ and $S_A^s(\vec{Q}, \omega)$ are time Fourier transforms of corresponding intermediate scattering functions, i.e.,

$$S_{AB}(\vec{Q}, \omega) = \frac{1}{2\pi} \int_{-\infty}^{\infty} dt \exp(-i\omega t) F_{AB}(\vec{Q}, t), \quad (3a)$$

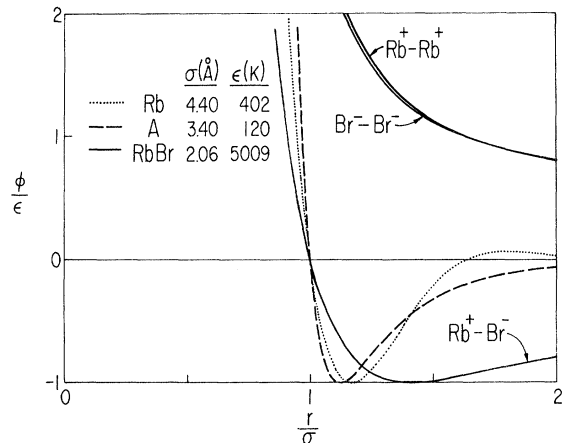


FIG. 1. Scaled interatomic potentials for Ar, Rb, and RbBr. Values for the scaling parameters are given in the figure.

$$S_A^s(\vec{Q}, \omega) = \frac{1}{2\pi} \int_{-\infty}^{\infty} dt \exp(-i\omega t) F_A^s(\vec{Q}, t), \quad (3b)$$

where (cf. Ref. 10)

$$F_{AB}(\vec{Q}, t) = (N_A N_B)^{-1/2} \times \sum_i^{N_A} \sum_j^{N_B} \langle \exp[-i\vec{Q} \cdot \vec{R}_{Ai}(0)] \exp[i\vec{Q} \cdot \vec{R}_{Bj}(t)] \rangle \quad (4a)$$

and

$$F_A^s(\vec{Q}, t) = N_A^{-1} \sum_i^{N_A} \langle \exp[-i\vec{Q} \cdot \vec{R}_{Ai}(0)] \exp[i\vec{Q} \cdot \vec{R}_{Ai}(t)] \rangle. \quad (4b)$$

Here $\vec{R}_{Ai}(t)$ is the position vector operator, for the i th atom of type A , at time t . Time-dependent pair correlation functions¹¹ are then given by

$$G_{AB}(\vec{r}, t) = \frac{1}{(2\pi)^3} \int d\vec{Q} \exp(-i\vec{Q} \cdot \vec{r}) F_{AB}(\vec{Q}, t) \\ = (N_A N_B)^{-1/2} \sum_i^{N_A} \sum_j^{N_B} \int d\vec{r}' \langle \delta(\vec{r} - \vec{r}' + \vec{R}_{Ai}(0)) \delta(\vec{r}' - \vec{R}_{Bj}(t)) \rangle \quad (5a)$$

and

$$G_A^s(\vec{r}, t) = \frac{1}{(2\pi)^3} \int d\vec{Q} \exp(-i\vec{Q} \cdot \vec{r}) F_A^s(\vec{Q}, t) \\ = N_A^{-1} \sum_i^{N_A} \int d\vec{r}' \langle \delta(\vec{r} - \vec{r}' + \vec{R}_{Ai}(0)) \delta(\vec{r}' - \vec{R}_{Ai}(t)) \rangle. \quad (5b)$$

In the classical limit $G_{AB}(\vec{r}, t)$ represents the probability of finding an atom of type A at position \vec{r} at time t , given there was an atom of type B at the origin at time $t=0$, whereas $G_A^s(\vec{r}, t)$ gives the probability of finding an atom of type A at position \vec{r} at time t , given that the same atom was at the origin at time $t=0$. At time $t=0$ we may write

$$G_{AB}(\vec{r}, 0) = \delta_{AB} \delta(\vec{r}) + (\rho_A \rho_B)^{1/2} g_{AB}(\vec{r}) \quad (6a)$$

and

$$G_A^s(\vec{r}, 0) = \delta(\vec{r}), \quad (6b)$$

where ρ_A is the mean number density of atoms of type A , and $g_{AB}(\vec{r})$ is a radial distribution function. With the above definitions we obtain

$$\langle \omega_{AB}^0 \rangle = S_{AB}(\vec{Q}) + (N_A N_B)^{1/2} \delta_{\vec{Q}, 0}, \quad (9a)$$

$$\langle \omega_A^0 \rangle^s = 1, \quad (9b)$$

$$\langle \omega_{AB}^2 \rangle = Q^2 k_B T \delta_{AB} / M_A, \quad (10a)$$

$$\langle \omega_A^2 \rangle^s = Q^2 k_B T / M_A, \quad (10b)$$

$$\langle \omega_{AB}^4 \rangle = \frac{Q^2 k_B T}{M_A M_B} \left[\delta_{AB} \left(3Q^2 k_B T + \sum_C^n \rho_C \int d\vec{r} g_{AC}(\vec{r}) \frac{\partial^2 \phi_{AC}(\vec{r})}{\partial x^2} \right) - (\rho_A \rho_B)^{1/2} \int d\vec{r} g_{AB}(\vec{r}) \cos(\vec{Q} \cdot \vec{r}) \frac{\partial^2 \phi_{AB}(\vec{r})}{\partial x^2} \right], \quad (11a)$$

$$\langle \omega_A^4 \rangle^s = \frac{Q^2 k_B T}{M_A^2} \left(3Q^2 k_B T + \sum_C^n \rho_C \int d\vec{r} g_{AC}(\vec{r}) \frac{\partial^2 \phi_{AC}(\vec{r})}{\partial x^2} \right). \quad (11b)$$

In these expressions k_B is Boltzmann's constant, T is the temperature, M_A is the mass of an atom of type A , and $\phi_{AB}(\vec{r})$ is the potential between an atom of type A and an atom of type B .

$$S_{AB}(\vec{Q}) \equiv F_{AB}(\vec{Q}, 0) - (N_A N_B)^{1/2} \delta_{\vec{Q}, 0} \\ = \delta_{AB} + (\rho_A \rho_B)^{1/2} \int d\vec{r} \exp(i\vec{Q} \cdot \vec{r}) [g_{AB}(\vec{r}) - 1]. \quad (7)$$

This equation defines the partial structure factors $S_{AB}(\vec{Q})$. Note that the definition given here differs from that of Faber and Ziman.¹² The moments of the scattering functions are defined by the equations

$$\langle \omega_{AB}^n \rangle \equiv \int_{-\infty}^{\infty} d\omega \omega^n S_{AB}(\vec{Q}, \omega), \quad (8a)$$

$$\langle \omega_A^n \rangle^s \equiv \int_{-\infty}^{\infty} d\omega \omega^n S_A^s(\vec{Q}, \omega). \quad (8b)$$

For a classical system the odd moments vanish. The zeroth, second, and fourth moments are

For an isotropic system only the magnitudes of \vec{r} and \vec{Q} are important. Furthermore, it is sometimes convenient to define "symmetrized" scattering functions by writing

$$\tilde{S}_{AB}(Q, \omega) = \exp(\hbar\omega/2k_B T) S_{AB}(Q, \omega), \quad (12)$$

and similarly for $\tilde{S}_A^*(Q, \omega)$, where $\hbar\omega$ is the energy gained by the neutron.

One can define linear combinations of the partial scattering functions which describe fluctuations of quantities such as number density, charge density, or mass density. For an ionized system especially useful quantities are the total number density

$$\rho(\vec{r}, t) = \sum_A \rho_A(\vec{r}, t) \quad (13)$$

and total charge density

$$Q(\vec{r}, t) = \sum_A Z_A \rho_A(r, t), \quad (14)$$

where $Z_A e$ are the ionic charges. In a two-component system the three appropriate scattering functions are given by

$$\rho S_{NN} = \rho_1 S_{11} + 2(\rho_1 \rho_2)^{1/2} S_{12} + \rho_2 S_{22}, \quad (15a)$$

$$\rho S_{NQ} = \rho_1 Z_1 \{ S_{11} + [(\rho_2/\rho_1)^{1/2} - (\rho_1/\rho_2)^{1/2}] S_{12} - S_{22} \}, \quad (15b)$$

$$\rho S_{QQ} = (\rho_1 Z_1)^2 [S_{11} \rho_1^{-1} - 2S_{12} (\rho_1 \rho_2)^{-1/2} + S_{22} \rho_2^{-1}]. \quad (15c)$$

Analogous intermediate scattering functions [Eq. (4)] and pair-correlation functions [Eq. (5)] can be defined. In a two-component system with equal numbers of two components of charges $\pm e$, Eq. (15) becomes

$$S_{NN} = \frac{1}{2}(S_{11} + S_{22}) + S_{12}, \quad (16a)$$

$$S_{NQ} = \frac{1}{2}(S_{11} - S_{22}), \quad (16b)$$

$$S_{QQ} = \frac{1}{2}(S_{11} + S_{22}) - S_{12}, \quad (16c)$$

and the coherent scattering cross section [Eq. (2a)] becomes

$$\left. \frac{d^2\sigma}{d\Omega dE_1} \right|_{\text{coh}} = \frac{k_1}{4\hbar k_0} [(b_1 + b_2)^2 S_{NN} + 2(b_1^2 - b_2^2) S_{NQ} + (b_1 - b_2)^2 S_{QQ}], \quad (17)$$

where the angular brackets round the b_i have been dropped for convenience. Clearly S_{NN} and S_{QQ} are measured if $b_1 = \pm b_2$, respectively. In the present experiment the first condition is approximately satisfied.

III. MEASUREMENTS AND DATA REDUCTION

The measurements were made with the hybrid time-of-flight spectrometer¹³ at the Argonne CP-5 reactor. Two series of runs were made, with incident neutron energies (E_0) of 4.96 and 32.9

meV and over-all energy resolutions full width at half maximum (FWHM) of 0.25 and 1–1.2 meV, respectively. We shall refer to these as experiments 1 and 2.

For experiment 1, with $E_0 = 4.96$ meV, measurements were made with detector groups centered about 31 values of the scattering angle ranging from 27.6° to 115.2° (corresponding to wave-vector transfers Q varying from 0.7 to 2.6 Å⁻¹ at zero energy transfer). Single detectors were used between 81.6° and 94.8°, corresponding to Q values near the peak of the structure factor $S_{NN}(Q)$ (see Sec. IV below). Groups of two or three adjacent detectors were used elsewhere. Time-analyzed data for each detector group were collected in 128 time channels of width 20 μsec, covering a range of scattered energies (E_1) from 3.4 to ~100 meV.

For experiment 2, with $E_0 = 32.9$ meV, the detector groups were centered at 31 scattering angles from 27.0° to 118.8°, corresponding to a range in Q of 1.9 to 6.9 Å⁻¹ at zero energy transfer. Groups of two or three adjacent detectors were used. Data were collected in 128 time channels of width 10 μsec, covering a range in E_1 of 10.7 to ~140 meV.

The sample material was "polaro-grade" RbBr powder prepared by Dr. S. Anderson at the University of Illinois. The material had been kept in an inert atmosphere since preparation from the melt. According to specifications, impurity metal ions were present to less than 200 ppm and other impurities (OH⁻, SO₄⁻, H₂O) to less than 10 ppm. The powder was contained in a tantalum tube of i.d. 1.488 cm and o.d. 1.590 cm. Tantalum was chosen for its good mechanical properties at high temperatures and its resistance to corrosion by the molten salt. The bottom cup was heliarc welded onto the tube, which was then placed in a glove box with an inert atmosphere, where the sample was loaded and the top welded on. In experiment 1, the tube also contained an array of boron nitride disks, 1.59 cm apart, 0.089 cm thick, mounted on a thin tantalum rod. The boron nitride disks acted as absorbing spacers to reduce multiple scattering. Subsequent studies with the multiple scattering program MSCAT (see below) indicated that these disks were not necessary: they were not used in experiment 2 (see also Ref. 17 of Ref. 3). The sample weight was 43.82 g in experiment 1 and 47.14 g in experiment 2. At a density¹⁴ of 2.682 g cm⁻³ for the liquid at 986 K these weights correspond in both cases to sample heights slightly greater than the beam height of 10 cm.

The furnace is illustrated in Fig. 2. The sample is heated by radiation from a resistively heated coil of tantalum wire 0.05 cm thick, wound round a boron nitride column placed to one side of the

sample, away from both the incident beam and the beams scattered to the detectors. A boron nitride pedestal attached to the bottom of the column, and a boron nitride collar attached to its top, supported the sample container. The whole assembly was surrounded by a single radiation shield of molybdenum sheet 0.0025 cm thick. The temperature was controlled and measured by means of two thermocouples attached to the boron-nitride pedestal and collar. The melting of the sample was followed by observing the behavior of the elastic scattering as the sample was heated. Melting was observed to take place between 943 K and 953 K as measured by the thermocouples, compared with reported values^{14, 15} in the range 953–965 K. The measurements were made at a measured temperature of 986 ± 10 K, to ensure that all the sample was molten.

A number of different runs have to be made in order to obtain corrected normalized data in a liquid experiment, as discussed in Ref. 16. In experiment 1, runs were made: (i) with the empty sample container at 986 K (9023 min), (ii) with the RbBr sample at the same temperature (17319 min), (iii) with a vanadium slab covering the same beam area (two runs for 2427 and 2334 min), and (iv) with no sample, and a 1- μ sec time channel width to determine timing parameters (61 min). In experiment 2, the same types of run were made (9239 min for the empty container, 9188 min for the sample, 2040, 2231, and 1898 min for three vanadium runs, and 70 min for the timing run). In addition, a "no sample" run (2146 min) was performed using the vanadium holder, in order to correct for a small amount of Bragg scattering obtained at the shorter wavelength from a boron nitride absorber plate placed after the sample position. In experiment 2, time-independent backgrounds were measured for each detector by placing a Cd shutter in the beam for 1 min in every 30 and recording the integrated count. At the time of experiment 1 this facility was not available, and time-independent backgrounds were obtained from averages of the first 10 time channels for each detector, which corresponded to energy transfers large enough that the inelastic scattering could be neglected.

The data analysis for each experiment closely followed the procedure used for Rb, as described in detail in Ref. 3. The empty container data were multiplied by a sample attenuation factor¹⁶ which was independently calculated for all detector groups and time channels. Values ranged from 0.76 to 0.84 in experiment 1 and from 0.85 to 0.88 in experiment 2. The empty container data were then normalized to the sample run and subtracted. The resulting counts were then normalized using

the vanadium runs to give an "uncorrected" symmetrized scattering function $\bar{S}(Q, \omega)$. (The absence of any subscript implies that we are describing a measured function.)

The multiple scattering correction was computed using the program MSCAT.¹⁷ In these experiments the correction was complicated because of the sizeable scattering from the tantalum container, which had to be considered in the multiple scattering calculations. Kernels for the scattering from both sample and container were thus required. For the sample, a model was used analogous to that derived by Pathak and Singwi,¹⁸ but generalized to a two-component system. The parameters of the model were obtained by fitting to the moments $\langle \omega_{AB}^0 \rangle$, $\langle \omega_{AB}^2 \rangle$, and $\langle \omega_{AB}^4 \rangle$. The zeroth and fourth moments were obtained from the molecular-dynamics calculations reported in II. For a series of values of Q , in the range from 0.1 to 20 \AA^{-1} , parameters of the Pathak-Singwi type¹⁸ were obtained by fitting to the moments, and then used to generate model values for the functions $S_{AB}(Q, \omega)$ for $0 \leq \omega \leq 200$ psec⁻¹. The kernel for the scattering from the sample container was derived in the incoherent approximation using the harmonic force constants for tantalum obtained by Woods.¹⁹ Multiphonon processes were included to all orders.

Strictly speaking, multiple scattering corrections should be made for both empty sample container and sample runs (see Ref. 16). However, when these corrections were calculated using the

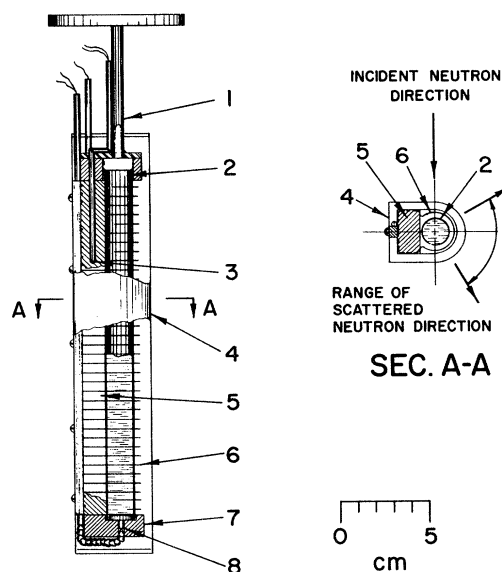


FIG. 2. Sketch of the heater and sample container configuration. Legend: 1, stainless-steel tube; 2, Ta sample container; 3, 8, thermocouples; 4, Mo radiation shield; 5, BN column; 6, Ta heater wire; 7, BN pedestal.

MSCAT program, it turned out that the multiple scattering correction for the empty container run was negligible except for a few time channels in the elastic scattering region. On the other hand, the experimental scattering function showed no anomalous behavior in this region, indicating that the elastic scattering from the sample container was adequately removed from the data. The multiple scattering correction to the empty container run was therefore neglected, and the correction for the sample run was computed over a grid of energy transfers which did not include a value exactly at zero. The ratios of total to single scattering varied from 1.02 to 1.80 for experiment 1 and from 1.013 to 2.20 for experiment 2, being a sharply increasing function of energy transfer in both cases.

After subtracting the multiple scattering correction, the self-shielding correction¹⁶ was applied, calculated independently for all detector groups and time channels using an energy-dependent scattering cross section computed from the kernel by MSCAT. Values of the correction factor ranged from 0.46 to 0.55 in experiment 1 and from 0.67

to 0.70 in experiment 2. The resolution correction was then made with the program RESOLV,¹⁶ using resolution parameters measured in the vanadium run. This procedure yielded corrected absolute values for the symmetrized scattering function $\tilde{S}(Q, \omega)$ and for the intermediate scattering function $F(Q, t)$ (Sec. II).

IV. RESULTS AND DISCUSSION

Selected results for $\tilde{S}(Q, \omega)$, obtained from experiments 1 and 2, are shown in Figs. 3 and 4, respectively. To give the reader a feel for the quality of the data, we show the experimental points prior to the resolution correction, together with the functions fitted by the program RESOLV,¹⁶ both before and after the correction for resolution. It can be seen that the correction was extremely small in these experiments, essentially because of the high sample temperature, which implies (through the second moment relation) relatively broad distributions for $\tilde{S}(Q, \omega)$. The $\tilde{S}(Q, \omega)$ plots show the increasing width in ω with increasing Q which is expected from the second moment rela-

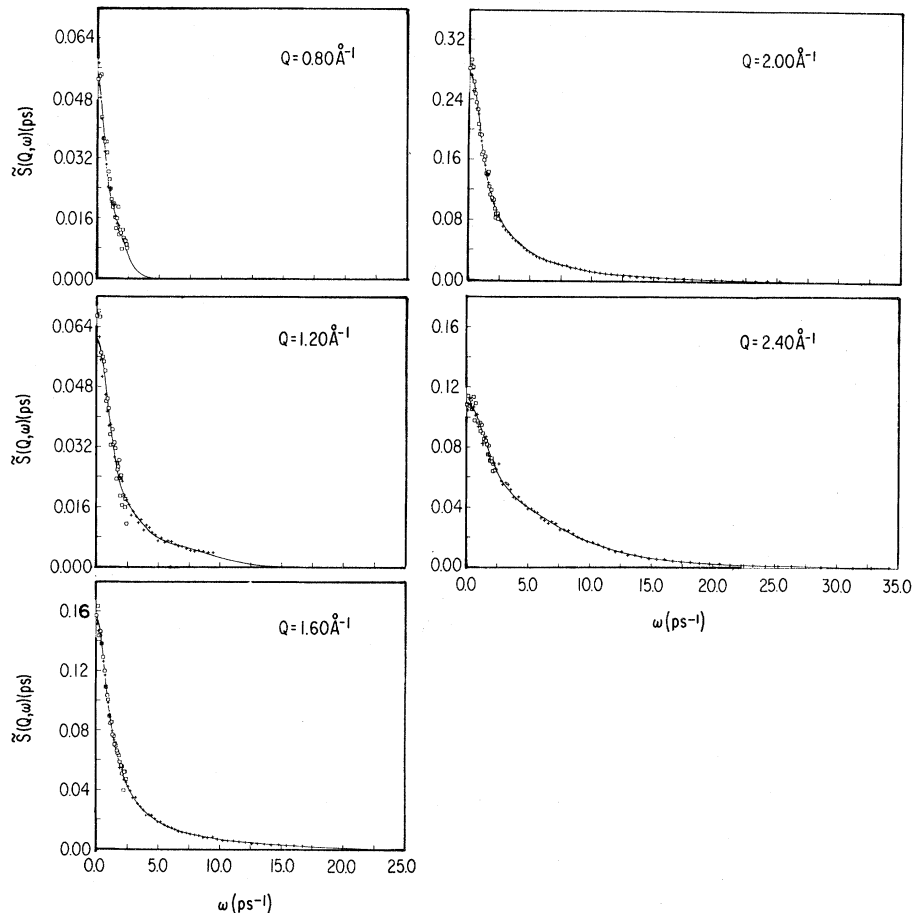


FIG. 3. Symmetrized scattering function $\tilde{S}(Q, \omega)$ for five values of Q , obtained from experiment 1. The points show the experimental data, without resolution correction, for neutron energy loss (\square) and energy gain ($+$). The two continuous curves show the fitted functions before and after resolution correction. For $Q=0.8 \text{ \AA}$ and 1.2 \AA the fitted function falls off too rapidly, due to the restricted range of the data, as discussed in the text.

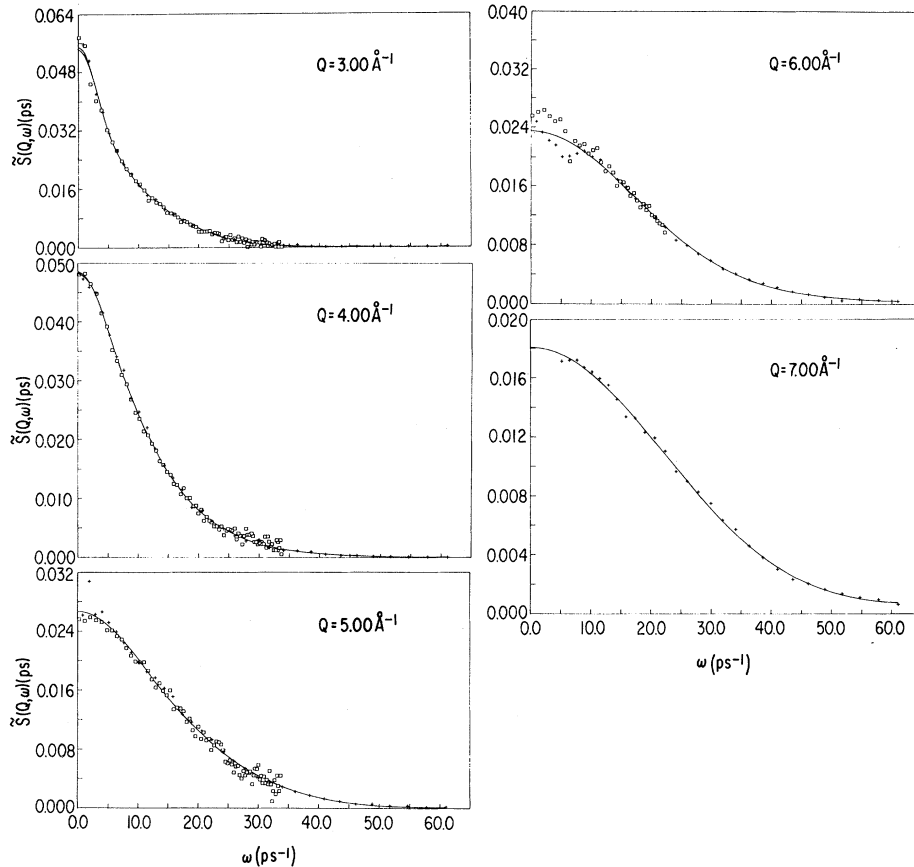


FIG. 4. Symmetrized scattering function $\hat{S}(Q, \omega)$ for five values of Q , obtained from experiment 2. Notation is the same as for Fig. 3.

tion. For smaller values of Q the curves display a characteristic peaked distribution for small ω , followed by a long tail for large ω , whereas for larger Q the curves go over to the Gaussian independent-particle shape. Both these features are consistent with the fourth-moment relation,²⁰ as discussed more quantitatively below.

An independent check on the reliability of the data is obtained from a comparison of the energy gain and energy loss measurements. As is seen in Figs. 3 and 4, the agreement is good except for the smaller ω values at $Q = 6.0 \text{ \AA}^{-1}$, where there were problems correcting for the sample container scattering.

In Figs. 5 and 6 we show corresponding plots of $F(Q, t)$ obtained from the program RESOLV.¹⁷ Only the real part of $F(Q, t)$ is plotted since the imaginary part is negligible at high temperatures.

The experimental zeroth moment $S(Q)$ is shown in Fig. 7. At small values of Q it is likely to be slightly underestimated because our measurements did not extend to sufficiently large energy transfers. This point is discussed further in the following paragraph. The results from the two experiments are in good agreement in the region of over-

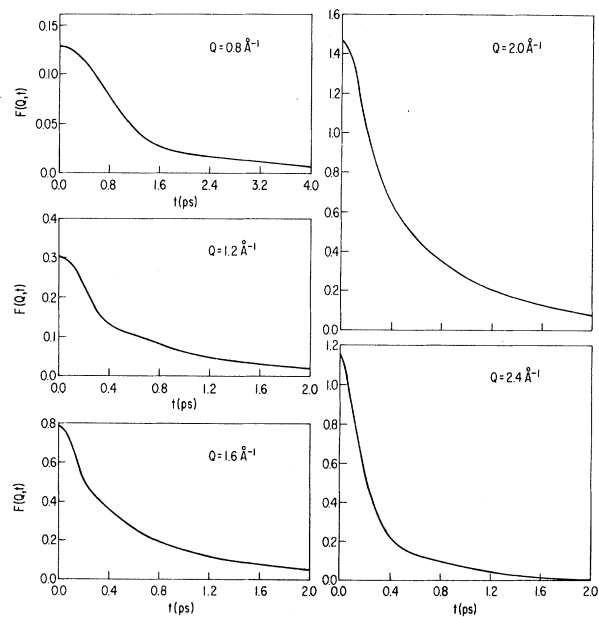


FIG. 5. Intermediate scattering function $F(Q, t)$ for five values of Q , obtained from experiment 1.

lap ($Q \sim 2.5 \text{ \AA}^{-1}$), but our data for larger values of Q appear to oscillate about an asymptotic value of about 1.04. This discrepancy could be caused by a number of factors, either singly or combined, such as errors in our values for the Debye-Waller factor $\exp(-2W)$ of vanadium²¹ or for the scattering lengths of Rb and Br, or slow variations in monitor efficiency during the experiment. Another possible reason for the discrepancy is our neglect of any incoherent scattering in the data analysis. Since the incoherent cross section is 0.24 ± 0.24 b per ion pair (see Table I), we should subtract a constant amount, 0.02 ± 0.02 , from our measured $S(Q)$. In view of the uncertainty in the incoherent scattering cross section of bromine, this correction did not seem to be justified.

The second moment $\langle \omega^2 \rangle$ of our experimental data, divided by the exact theoretical result (Sec. II), is shown in Fig. 8. At small values of Q the experimental moment is far too small, largely because our measurements did not extend far enough in ω . For a given Q , the maximum value of ω is obtained at the smallest angle in experiment 1, namely 27.6° . Thus for $Q = 1.2$ and 1.8 \AA^{-1} , for example, the maximum ω was 9.6 and 21.2 psec^{-1} ,

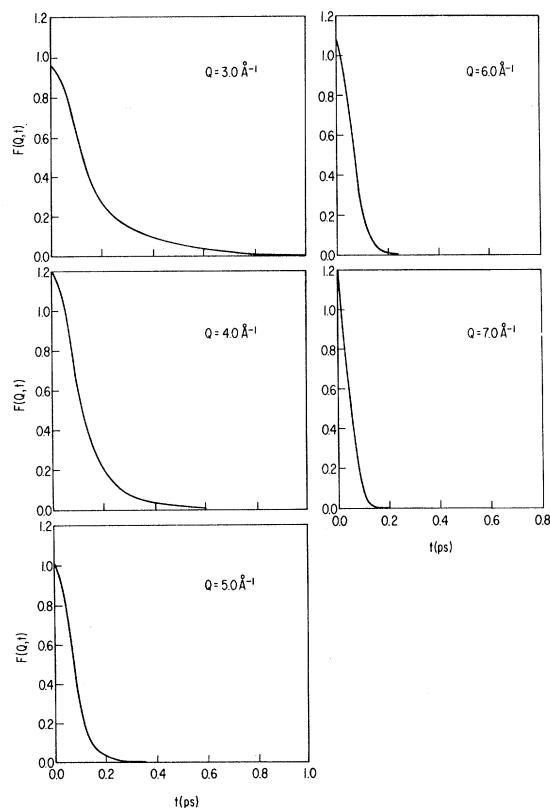


FIG. 6. Intermediate scattering function $F(Q,t)$ for five values of Q , obtained from experiment 2.

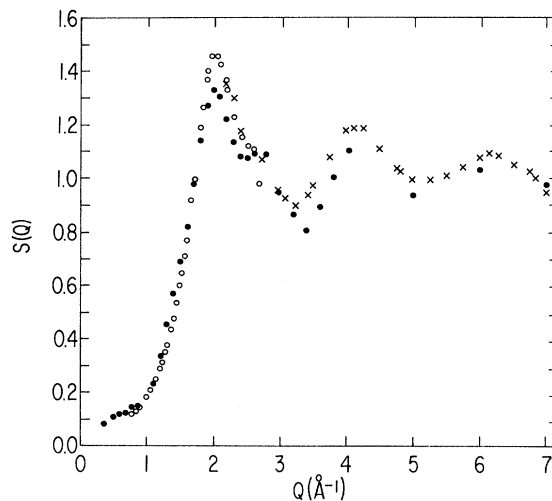


FIG. 7. Values for $S(Q)$ derived from the neutron experiments 1 (\circ) and 2 (\times) and from the molecular-dynamics calculations (\bullet).

respectively, whereas the maximum in $\omega^2 \bar{S}(Q, \omega)$ occurs at (very roughly) 15 and 10 psec^{-1} , respectively. Thus we cannot hope to evaluate $\langle \omega^2 \rangle$ for $Q \leq 1.5 \text{ \AA}^{-1}$, since the measurements do not even extend to the peak in $\omega^2 S(Q, \omega)$. For the same reason the functions fitted to the $\bar{S}(Q, \omega)$ data for $Q = 0.8 \text{ \AA}^{-1}$ and 1.2 \AA^{-1} fall off too rapidly (see Fig. 3). On the other hand, the results for $Q \geq 1.8 \text{ \AA}^{-1}$ extend far enough to allow a reasonably reliable evaluation of $\langle \omega^2 \rangle$. The experimental second moments do not agree very well in the region of overlap between experiments 1 and 2, and at larger Q values the results are too high. This may partly result from a normalization error of the type discussed above, but the remaining dis-

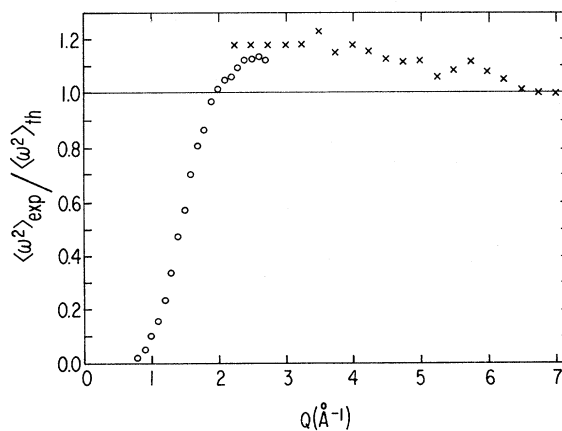


FIG. 8. Ratio of experimental to theoretical values of the second moment $\langle \omega^2 \rangle$. The symbols (\circ) and (\times) refer to experiments 1 and 2, respectively.

crepancy is probably due to uncertainties in the multiple scattering correction and/or the background subtraction.

There are other quantities which may be used to characterize the development of the scattering function with Q ; these include the full width at half-maximum (FWHM) and the central value $\tilde{S}(Q, 0)$. Further, one may consider the function

$$\tilde{C}(Q, \omega) \equiv \omega^2 \tilde{S}(Q, \omega), \quad (18)$$

which describes the current fluctuations in the system.²² [The integral of the corresponding unsymmetrized function at constant Q is the second moment $\langle \omega^2 \rangle$ of the scattering function $S(Q, \omega)$]. When $\tilde{C}(Q, \omega)$ is plotted against ω at constant Q , it must inevitably peak at some nonzero value of ω which we may call ω_m . Thus, two further functions which may be plotted against Q are ω_m and $\tilde{C}(Q, \omega_m) \equiv \omega_m^2 \tilde{S}(Q, \omega_m)$.

The variations of these four quantities with Q reflect the behavior of the structure factor $S(Q)$. To extract physical information from these data, it is desirable to remove some of this dependence on $S(Q)$. This can be achieved without relying on any particular model by comparing with a simple functional form for $\tilde{S}(Q, \omega)$ which has the correct area $S(Q)$ and correct variance

$$\omega_0^2(Q) = \langle \omega^2 \rangle / S(Q). \quad (19)$$

This is the equivalent Gaussian function given by

$$\tilde{S}_G(Q, \omega) = \frac{S(Q)}{(2\pi)^{1/2} \omega_0} \exp\left(\frac{-\omega^2}{2\omega_0^2}\right). \quad (20)$$

One can then define the following ratios, between the experimental values of the FWHM, $\tilde{S}(Q, 0)$, ω_m , and $\omega_m^2 \tilde{S}(Q, \omega_m)$, and the corresponding values for the equivalent Gaussian:

$$\frac{[\text{FWHM}]_{\text{expt}}}{[\text{FWHM}]_G} = \frac{[\text{FWHM}]_{\text{expt}}}{2(2 \ln 2)^{1/2} \omega_0}, \quad (21a)$$

$$\frac{[\tilde{S}(Q, 0)]_G}{[\tilde{S}(Q, 0)]_{\text{expt}}} = \frac{S(Q)/(2\pi)^{1/2} \omega_0}{[\tilde{S}(Q, 0)]_{\text{expt}}}, \quad (21b)$$

$$\frac{[\omega_m]_{\text{expt}}}{[\omega_m]_G} = \frac{[\omega_m]_{\text{expt}}}{\sqrt{2} \omega_0}, \quad (21c)$$

$$\frac{[\omega_m^2 \tilde{S}(Q, \omega_m)]_G}{[\omega_m^2 \tilde{S}(Q, \omega_m)]_{\text{expt}}} = \frac{\omega_0 S(Q) / (\pi/2)^{1/2} e}{[\omega_m^2 \tilde{S}(Q, \omega_m)]_{\text{expt}}}. \quad (21d)$$

In addition to these measured quantities, it is instructive to scale the function ω_i , given by

$$\omega_i^2 = \langle \omega^4 \rangle / \langle \omega^2 \rangle, \quad (22)$$

which characterizes the ratio of the fourth to the second moment, in a similar manner. This is done by noting that, for the equivalent Gaussian, $\omega_i^2 = 3\omega_0^2$, and therefore we define a fifth ratio

$$\omega_i / [\omega_i]_G = \omega_i / \sqrt{3} \omega_0. \quad (23)$$

Note, however, that in this case, ω_i is a calculated function obtained from Eqs. (22), (10a), and (11a) with values of the distribution functions $g_{AB}(r)$ obtained from molecular dynamics (paper II).

The ratios defined in Eqs. (21) and (23) are plotted in Fig. 9. We note that at smaller values of Q the measured values of the FWHM and $S(Q)/S(Q, 0)$ are lower than those of the equivalent Gaussian, whereas the values of the other ratios are higher. This is the characteristic behavior of a function which, relative to the Gaussian of the same area and variance, has a peaked low-frequency portion and a slowly decaying high-frequency portion. This shape is suggested visually by the curves in Fig. 3 and was, in fact, postulated for a general liquid by de Gennes²⁰ on the basis of the behavior of ω_i . In terms of the decay of the density fluctuations with time, it implies a rapid initial decrease of the amplitude of the fluctuation followed by a period in which it decays more slowly, a behavior which is relatively more pronounced near the peak of the structure factor. For larger values of Q the ratios approach unity as the scattering functions acquire the Gaussian shape corresponding to the independent-particle regime.

This type of behavior was also found in liquid Ar and Rb (Refs. 1 and 3, respectively) and appears to be common to all simple liquids. A comparison between different simple liquids therefore requires a detailed quantitative analysis in terms of specific theories, which will be given in a subsequent paper. Comparison of the data with recent theoretical work²³ will be given at the same time.

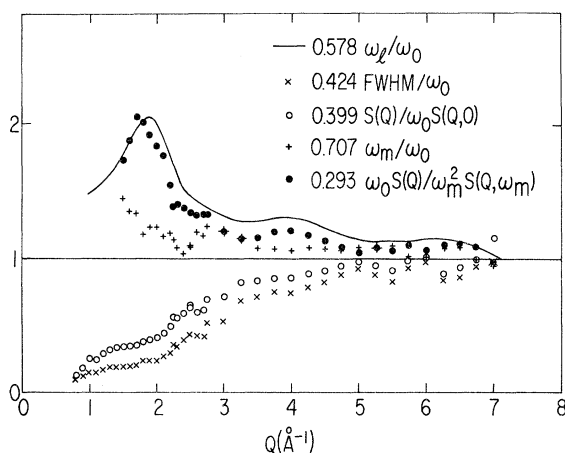


FIG. 9. Values of the functions defined in Eqs. (21) and (23) of the text.

ACKNOWLEDGMENTS

The authors thank R. Kleb, G. E. Ostrowski, and R. Stefiuk for valuable technical assistance. Useful discussions with M. Blander, D. Gruen, A. Rahman, J. M. Rowe, K. S. Singwi, K. Sköld, and M. Tosi are gratefully acknowledged.

- †Work performed in part under the auspices of the U. S. Atomic Energy Commission.
- ¹K. Sköld, J. M. Rowe, G. E. Ostrowski, and P. D. Randolph, *Phys. Rev. A* **6**, 1107 (1972); J. M. Rowe and K. Sköld, in *Neutron Inelastic Scattering 1972* (IAEA, Vienna, 1972), p. 413. Liquid neon has also been studied in considerable detail: W. J. L. Buyers, V. F. Sears, P. A. Lonngi, and D. A. Lonngi, in *Neutron Inelastic Scattering* (IAEA, Vienna, 1972), p. 399; W. J. L. Buyers, V. F. Sears, P. A. Lonngi, and D. A. Lonngi, *Phys. Rev. A* **11**, 697 (1975).
- ²A. Rahman, *Phys. Rev.* **136**, A405 (1964); L. Verlet, *Phys. Rev.* **159**, 98 (1967); **165**, 201 (1968); D. Levesque and L. Verlet, *Phys. Rev. A* **2**, 2514 (1970); D. Levesque, L. Verlet, and J. Kürkijarvi, *Phys. Rev. A* **7**, 1690 (1973).
- ³J. R. D. Copley and J. M. Rowe, *Phys. Rev. A* **9**, 1656 (1974).
- ⁴A. Rahman, *Phys. Rev. A* **9**, 1667 (1974).
- ⁵H. Bell, A. Kollmar, B. Alefeld, and T. Springer, *Phys. Lett.* **45A**, 479 (1973); H. Bell, H. Moeller-Wenghoffer, A. Kollmar, R. Stockmeyer, T. Springer, and H. Stiller, *Phys. Rev. A* **11**, 316 (1975). These papers describe measurements on liquid neon.
- ⁶J. R. D. Copley and J. M. Rowe, *Phys. Rev. Lett.* **32**, 49 (1974).
- ⁷A. Rahman, *Phys. Rev. Lett.* **32**, 52 (1974).
- ⁸J. R. D. Copley and A. Rahman (unpublished).
- ⁹M. P. Tosi and F. G. Fumi, *J. Phys. Chem. Solids* **25**, 45 (1964).
- ¹⁰W. Marshall and S. W. Lovesey, *Theory of Thermal Neutron Scattering* (Clarendon, Oxford, 1971).
- ¹¹L. van Hove, *Phys. Rev.* **95**, 249 (1954).
- ¹²T. E. Faber and J. M. Ziman, *Phil. Mag.* **11**, 153 (1964).
- ¹³R. Kleb, G. E. Ostrowski, D. L. Price, and J. M. Rowe, *Nucl. Instrum. Methods* **106**, 221 (1973).
- ¹⁴I. S. Yaffe and E. R. van Artsdalen, *J. Phys. Chem.* **60**, 1125 (1956); S. Zuca and M. Olteanu, *Rev. Roum. Chim.* **13**, 1567 (1968).
- ¹⁵*Selected Values of Chemical Thermodynamic Properties*, NBS Circ. No. 500 (U.S. GPO, Washington, D. C., 1952).
- ¹⁶J. R. D. Copley, D. L. Price, and J. M. Rowe, *Nucl. Instrum. Methods* **107**, 501 (1973); **114**, 411(E) (1974).
- ¹⁷J. R. D. Copley, *Comput. Phys. Commun.* **7**, 289 (1974). Copies of this program may be obtained from the Argonne Code Center, Argonne National Laboratory, Argonne, Illinois, 60439.
- ¹⁸K. N. Pathak and K. S. Singwi, *Phys. Rev. A* **2**, 2427 (1970).
- ¹⁹A. D. B. Woods, *Phys. Rev.* **136**, A781 (1964).
- ²⁰P. G. de Gennes, *Physica* **25**, 825 (1959).
- ²¹For this experiment we used $2W/Q^2 = 0.0073 \text{ \AA}^2$, the value obtained by G. Venkataraman, K. Usha Deniz, P. K. Iyengar, A. P. Roy, and P. R. Vijayaraghavan, *J. Phys. Chem. Solids* **27**, 1103 (1966), who estimated an error of $\pm 0.0004 \text{ \AA}^2$. An error of $\pm 5\%$ in $2W/Q^2$ leads to an error of about $\pm 1.3\%$ in the normalization, for $Q = 6 \text{ \AA}^{-1}$.
- ²²A. Rahman, in *Statistical Mechanics, New Concepts, New Problems, New Applications*, edited by S. A. Rice, K. F. Freed, and J. C. Light (University of Chicago Press, Chicago, 1972), p. 177.
- ²³M. C. Abramo, M. Parrinello, and M. P. Tosi, *J. Nonmetals* **2**, 57 (1974); **2**, 67 (1974).